Microporous Membranes of Isotactic Poly(4-methyl-1-pentene) from a Melt-Extrusion Process. I. Effects of Resin Variables and Extrusion Conditions

MATTHEW B. JOHNSON, GARTH L. WILKES

Virginia Tech, Polymer Materials and Interfaces Laboratory and Department of Chemical Engineering, Blacksburg, Virginia 24061

Received 18 September 2000; accepted 21 June 2001

ABSTRACT: A study utilizing isotactic poly(4-methyl-1-pentene) (PMP) was undertaken to investigate a three-stage process (melt-extrusion/annealing/uniaxial-stretching) (MEAUS) employed to produce microporous films. The results of this study will be reported in the course of two articles. In this first part, three PMP resins were melt-extruded into tubular films (blowup ratio; BUR = 1), where the resins each differ in weight-average molecular weight (M_w). Specific attention was focused upon the morphological and crystal orientation results as a function of the melt-relaxation times as influenced by the resin characteristics and the processing parameters. The results of a number of melt-extrusion conditions are presented. A stacked lamellar morphology was obtained in each case; however, the type of stacked lamellar morphology, planar or twisted, and the orientation state was found to depend upon both the resin characteristics, specifically M_w, and the melt-extrusion conditions. Atomic force microscopy and wide-angle X-ray scattering (WAXS) were the main techniques utilized to study the melt-extruded films, while oscillatory shear measurements, in conjunction with a Carreau–Yasuda analysis, aided in differentiating the melt-flow behavior of the three resins. © 2002 John Wiley & Sons, Inc. J Appl Polym Sci 83: 2095–2113, 2002

Key words: processing; melt-extrusion; poly(4-methyl-1-pentene); PMP; stacked lamellae

INTRODUCTION

Membranes possessing a microporous morphology have found a wide variety of commercial applications—for example, they are utilized in microfiltration, blood oxygenation, dialysis, and reciprocator membranes.[1–4] Such microporous membranes are generally composed of a polymeric matrix with pore sizes ranging from 0.001 to 10 μm, where the pores vary in terms of their uniformity and distribution within the membrane. It is also important that continuity of these pores occurs, for without connectivity, their applicability is limited.

To fabricate such microporous materials, a number of methods have been proposed.[5–10] These range from the swelling of a semicrystalline material followed by a later stretching and removal of the swelling solvent,[6,7] stretching (uniaxially and/or biaxially) of a polymer matrix containing filler particles that have poor adhesion to the matrix, which leads to cavitation of the matrix upon deformation[8–10] fibrilization by biaxial stretching such as those based on polytetrafluroethylene,[11] and, finally, by what will be denoted

Correspondence to: G. L. Wilkes (gwilkes@vt.edu).
Contract grant sponsor: Celgard Corp. LLC.

Journal of Applied Polymer Science, Vol. 83, 2095–2113 (2002)

DOI 10.1002/app.10164

in this article as an melt-extrusion/annealed/uniaxial stretching (MEAUS) method. This latter approach possesses three key stages that occur in the following order: tubular melt-extrusion (blowup ratio; BUR = 1), annealing, and uniaxial-stretching of the annealed film parallel to the machine direction (MD). The latter operation stage is of two steps whose conditions vary in terms of temperature and degree of stretch. This process method has led to commercialization of microporous materials based on high-density polyethylene (HDPE) and isotactic polypropylene (iPP).[12] Publications from our laboratory[13] have discussed the characteristic morphological textures induced in HDPE by this MEAUS technique. Specifically, the characteristic features of the morphological texture of such film materials have been discussed in addition to the process variables as well as the parameters of molecular weight/molecular weight distribution.

To achieve an appropriate microporous membrane by this approach, it is first necessary to develop a precursor film made by the tubular extrusion process that possesses a planar stacked lamellar semicrystalline texture. Crystallization under higher stress is thus essential, according to the Keller and Machin[14] model, for producing this morphology. This important and well-recognized morphological model suggests that an axial-directed stress in the melt, as controlled by the processing conditions, is essential for fibril nucleation. Accordingly, low extrusion stress during crystallization produces a twisted lamellar morphology that nucleates from a central fibril nucleus to form winding ribbonlike structures. In the former case, higher extrusion stress results in preferential *c*-axis orientation parallel to the MD, as observed via WAXS, whereas the lower stress material generally possesses, for example, in HDPE, some level of *a*-axis orientation in addition to *c*-axis orientation. In either case, the central fibril nucleus is parallel to the direction of flow (typically MD). Additionally, the resin characteristics (e.g., M_w and MWD) are critical in controlling rheological and associated relaxation behavior; therefore, these two variables also play an important role in the morphological development and level of crystal orientation. Knowledge of the molecular characteristics of the resins and the processing conditions to which these resins are subjected thus aids in understanding the molecular aspects of the melt prior to crystallization.[15,16]

If the planar stacked lamellar morphology can be achieved, there is the potential for that precursor to be later transformed into a microporous membrane by following the appropriate annealing and stretching procedures. However, while this can be achieved for HDPE as well as iPP, unpublished work from this laboratory found that similar procedures applied to isotactic poly(1-butene) (PB-1) could lead to a stacked lamellar structure, but good microporous membranes could not be easily developed from such precursors. In brief, it was speculated that this is because PB-1 does not possess an α_c transition, thereby not allowing the annealing procedure to suitably modify the morphological texture. Thus, when the material is drawn along the MD, splaying of the lamellar and its development into a microporous texture does not appreciably occur. This supposition regarding the α_c transition was therefore directed toward poly(4-methyl-1-pentene) (PMP) of isotactic form. The reason for selecting this particular system is that it possesses a distinct α_c transition and some evidence exists in the literature[17,18] that it can lead to a microporous structure via a similar uniaxial stretching process. However, this material has not been systematically studied taking into account both extrusion variables and resin variation. Hence, it was the purpose of this report to address the behavior of PMP in the MEAUS process while taking into account both resin and extrusion variables. This analysis will be accomplished through a series of two articles of which this is the first. This initial report will cover only the melt-extrusion process and its inducement of the precursor films possessing MD orientation. A second forthcoming article will address the annealing and stretching stages for selected precursor films.

EXPERIMENTAL

Materials

Molecular weight and distribution information for the three individual resins is given in Table I. Besides obvious molecular weight differences, resin A (high M_w) and resin C (low M_w) each possess the same amount of the comonomer 1-decene, about 3.2 wt %, while resin B was determined to have nearly double this amount, as measured via solution NMR.[19] The additional comonomer content of resin B will be shown later to influence the crystallinity and to slow the crys-

Table I Molecular Weight Characteristics for the Three PMP Resins Studied

Sample	M_n (kg/mol)	M_w (kg/mol)	M_w/M_n
Resin A	44.5	460	10.3
Resin B	58.0	360	6.2
Resin C	36.9	290	7.8

tallization kinetics, thereby allowing greater time for oriented melt relaxation. In addition, one must also take into account the state of extrusion stress and the characteristic melt-relaxation time of the resin.

Melt Rheological Characterization

The resin samples were compression-molded at 270°C for a total time of 10 min. The samples were allowed to melt without pressure for 4 min and then subjected to a low molding pressure for an additional 6 min. The molded samples were subsequently quenched to ambient conditions upon removal from the press. The 25.4-mm-diameter compression-molded disks were of 2 mm in thickness. The modulus of the complex viscosity ($|\eta^*|$) as a function of frequency (ω) in radians/s was obtained by an RMS Rheometrics 800 spectrometer using a parallel-plate geometry. The rheometer test chamber was operated with a nitrogen atmosphere to minimize polymer degradation. The rheometer was preheated to the testing temperature of 270°C and allowed to reach thermal equilibration, before specimen loading of the specimens. The samples were squeezed between the plates to a thickness of 1.5 mm, at which time the excess sample was trimmed. A total of 10 min elapsed from the sample insertion and trimming to initiating the frequency sweep. The $|\eta^*|$ versus ω data were curve-fitted using the modified three-parameter Carreau–Yasuda (CY) model (Eq. 1) to obtain the CY parameters: η_0, the zero shear viscosity; the parameter a, which describes the severity or sharpness of the transition from Newtonian to shear-thinning behavior; and τ_n, the characteristic melt-relaxation time, correlated to the frequency where shear thinning begins. The power-law number (n) was set equal to 2/11, a value which was first proposed by Graessely in 1967,[20,21] based upon a theoretical model of polymer-chain disentanglement for narrow MWD systems. Characterization of the PMP rheological data in this article will also utilize a value of 2/11, since this choice applied well to our results as will be shown later. Further details regarding the CY model may be found elsewhere[22,23]:

$$|\eta^*(\omega)| = \frac{\eta_0}{[1 + (\omega\tau_n)^a]^{(1-n)/a}} \quad (1)$$

Tubular Film Processing

All the tubular 1-mil (25-μm) film samples were made on a laboratory scale: MPM brand extruder with a 3-in. (76-mm) annular die, a die gap of 0.070 in. (1.8 mm), and a single screw with a 1.5-in. (37.5-mm) diameter (aspect ratio, L/D = 36). The blowup ratio was maintained at unity, thereby promoting only planar extensional flow with the deformation direction along the MD. This leads to the expected result of uniaxial symmetry about the MD,[13] as will be verified later by WAXS and refractometry. The extruded melt was quenched with a single-lip Western air-ring system using ambient air at about 25°C. A schematic of the tubular film extruder is shown in Figure 1 with the important features labeled with the extrusion conditions employed. Four main processing parameters—extruder barrel temperature, T_{melt}; extrusion speed of the screw in revolutions per minute (rpm); quench height, the distance from the die exit to the cooling ring; and the line speed in meters per minute (mpm)—are listed with the specific conditions utilized in Tables

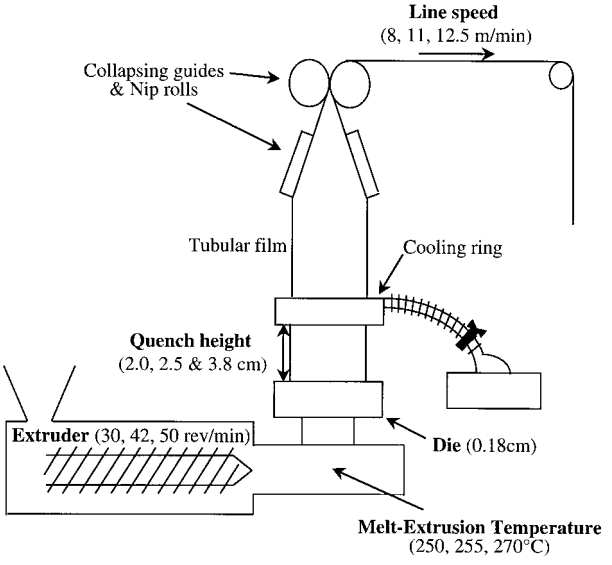

Figure 1 Schematic depicting the tubular extrusion setup utilized in this study with some processing parameters indicated.

Table II Summary of Melt-extrusion Conditions for Resin A

Extrusion Condition	Sample	Melt Temperature (°C)	Extrusion Speed (rpm)	Quench Height (cm)	Line Speed (mpm)
#1	A1	255	42	2.5	11
#2	A2	270	30	2.5	8
#3	A3	250	42	2.5	11
#4	A4	255	42	3.8	11

II–IV for resins A–C, respectively. In all cases, the line speed was adjusted to maintain a nominal film thickness of 1 mil (25 microns). Further, the flow rate of the air through the air ring was kept constant in this study, although a previous publication from this laboratory investigated this variable utilizing a similar extrusion scheme for HDPE.[13]

Structural and Optical Techniques Utilized

Wide-Angle X-ray Scattering (WAXS)

WAXS studies were performed on a Philips tabletop X-ray generator Model PW1720 equipped with a standard vacuum-sealed Warhus photographic pinhole camera. The X-ray beam was of CuKα radiation, $\lambda = 1.544$ Å, and was collimated to a beam diameter of 0.020 in. (0.508 mm).

In determining a quantitative value for orientation, the angular deviation of the average chain axis with respect to a specified reference axis is measured. A commonly reported parameter for uniaxially oriented systems is a second moment average, termed the Hermans' orientation, and is expressed by eq. (2) (Ref. 24):

$$f_H = \frac{(3\overline{\cos^2\theta} - 1)}{2} \tag{2}$$

The quantity $\overline{\cos^2\theta}$ represents the average value of $\cos^2\theta$ taken over all the polymer chains within the system or phase being measured. The value for θ is the angle between the average chain axis and the chosen reference axis. Therefore, if all the chains are perfectly oriented along the reference direction, then $\theta = 0°$ and $f_H = 1$. In contrast, if all chains are oriented perpendicular to that of the reference direction, then $\theta = 90°$ and $f_H = -1/2$. It can be shown for random orientation that $f_H = 0$.

Often, a common means used to determine f_H for the crystalline orientation of a material is via WAXS. In the PMP crystalline phase, the c-axis unit-cell orientation is often desirable because it directly correlates to the chain axis orientation. For melt-crystallized PMP, the unit cell is tetragonal ($a = b = 18.66$ Å and $c = 13.80$ Å).[25,26] Figure 2 depicts the coordinate system used to define a tetragonal unit cell with respect to a given set of orthogonal (x, y, z) axes. The angles α, β, and ε are measured with respect to the reference axis, z-axis or MD, and the a, b, and c unit-cell axes.

In the case of a tetragonal unit cell and uniaxial symmetry, both a-axis and b-axis orientation are equal; thus, f_a equals f_b ($\alpha = \beta$), leading to

$$2f_a + f_c = 0 \tag{3}$$

Hence, only a single reflection that is solely dependent on the a-axis ($h00$), b-axis ($0k0$), or c-axis (001) is required to follow the crystal orientation. For uniaxially oriented PMP materials, the set of planes typically followed is of the (200)

Table III Summary of Melt-extrusion Conditions for Resin B

Extrusion Condition	Sample	Melt Temperature (°C)	Extrusion Speed (rpm)	Quench Height (cm)	Line Speed (mpm)
#1	B1	255	42	2.5	11
#2	B2	270	30	2.5	8
#3	B3	250	42	2.5	11
#4	B4	255	42	3.8	11

Table IV Summary of Melt-extrusion Conditions for Resin C

Extrusion Condition	Sample	Melt Temperature (°C)	Extrusion Speed (rpm)	Quench Height (in.)	Line Speed (fpm)
#1	C1	255	42	2.5	11
#2	C2	270	30	2.5	8
#3	C3	250	42	2.5	11
#5	C5	250	52	2.0	12.5

planes.[27–29] Hermans' orientation function can be shown[30] to become

$$f_{200} = \frac{(3\ \cos^2\theta_{200}\overline{\sin^2\psi_{200}} - 1)}{2} \qquad (4)$$

where the azimuthal dependence of the scattered intensity for the (200) reflection is defined by the angle ψ_{200}, and θ_{200} is the Bragg angle. The quantity $\sin^2\psi_{hkl}$ is calculated by determining the scattering intensity of the appropriate scattering reflection as a function of the angle. It is represented by the following relationship:

$$\overline{\sin^2\psi_{200}} = \frac{\int_0^{\pi/2} I(\psi)\sin^2\psi_{200}\cos\ \theta_{200}\, d\psi}{\int_0^{\pi/2} I(\psi)\cos\ \theta_{200}\, d\psi} \qquad (5)$$

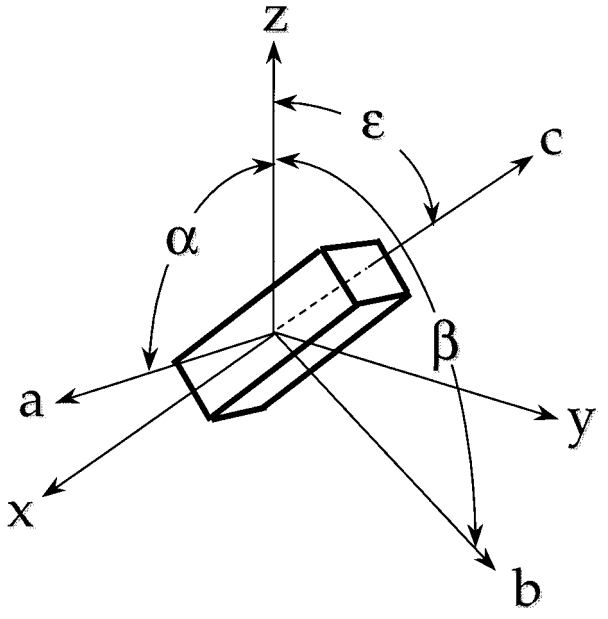

Figure 2 Coordinate system used to define the tetragonal unit cell with respect to a given set of orthogonal axes.

where $I(\psi_{200})$ is the relative intensity at the angle ψ_{200} for the (200) reflection. Equation (5) can also be evaluated graphically,[30–32] or $\sin^2\psi_{hkl}$ may be approximated by measuring the half-width of the (200) reflection.[29–32] Thus, the crystalline orientation can be estimated by examination of the azimuthal angle dependence of the (200) reflection obtained from standard flat-plate WAXS patterns.

Refractometry

To determine the refractive index in all three dimensions, that is, MD, transverse direction (TD), and normal direction (ND), a METRICON prism coupler refractometer Model 2010, equipped with a polarized laser, was utilized.[33]

Atomic Force Microscopy (AFM)

AFM micrographs were obtained using a Digital Instruments Nanoscope III scanning probe microscope operated in TappingMode™. Nanosensor TESP single-beam cantilever tips possessing force constants of 35 ± 7 N/m and oscillated at frequencies of about 290 kHz were used. The films were placed upon glass slides using double-stick tape. Raster scanning was done parallel to the film MD.

Transmission Electron Microscopy (TEM) and Scanning Electron Microscopy (SEM)

TEM micrographs were taken with a Philips EM-420 scanning transmission electron microscope (STEM) operated in the transmission mode at 100 kV. Samples were prepared by staining with RuO_4 to increase the electron density of the amorphous phase, thus providing sufficient contrast between the amorphous and crystalline phases. Prior to staining, the films were embedded in epoxy, which was cured at room temperature overnight. Thin sections were then microtomed at room temperature using a diamond knife on a Reichert–Jung Cryo-

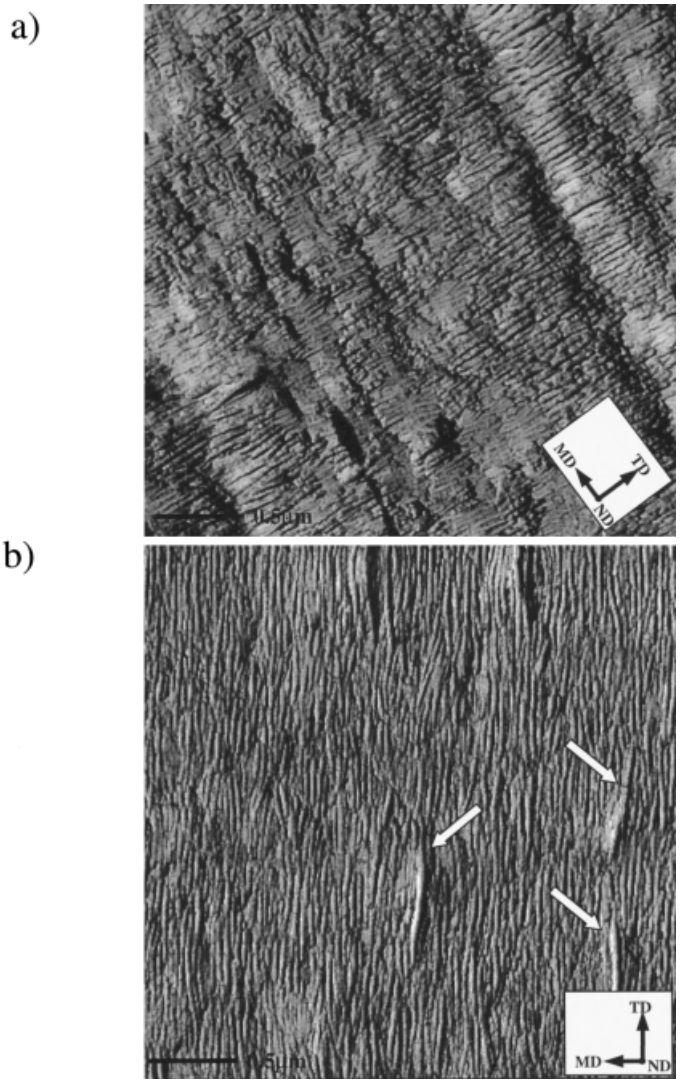

Figure 3 AFM phase images of the resin A PMP films: (a) A1; (b) A2; (c) A3; (d) A4. The MD is labeled. Images are 3 × 3 μm.

ultramicrotome Ultracut E. Vapor staining was next performed at ambient using 10-mL aliquots of 0.5 wt % RuO_4 staining solutions. First, the staining solution was placed with the sample in the staining vessel until sufficient time had elapsed such that no further vapor staining occurred (ca. 3 h). After that period of time, the initial solution was replaced with a fresh 10-mL aliquot of RuO_4. This was repeated three to four times (i.e., a total of 30–40 mL was used). As a result of the staining, the micrographs display darkened amorphous regions and lighter crystalline lamella. SEM analysis was also performed on selected films with a LEO 1530 field emission SEM utilizing low voltages (ca. 1–3 kV) to reduce beam damage.

Differential Scanning Calorimetry (DSC)

DSC measurement was performed with a Perkin–Elmer DSC-7 operating at a cooling rate of 30°C/min utilizing sample weights of about 5 mg. Sample temperatures were increased to 270°C for 10 min, followed by cooling to follow crystallization. The samples were then reheated to 270°C for 15 min followed by a second crystallization. It is noted that the results of both cooling scans were analogous. All DSC scans were performed under a N_2 atmosphere. Heating scans were also conducted utilizing a heating rate of 30°C/min with a sample weight of about 5 mg. The mass fraction of crystallinity using DSC was calculated from the following mass fraction relationship:

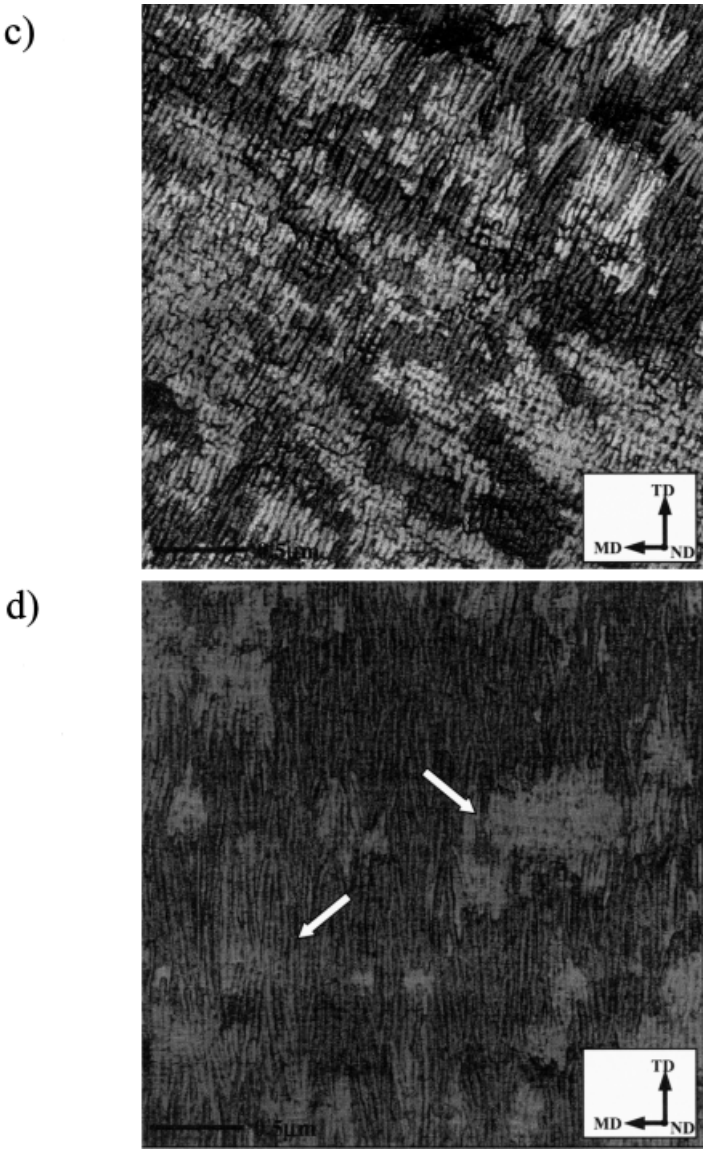

Figure 3 (*Continued from the previous page*)

$$X_c = \frac{\Delta H_f}{\Delta H_f^0} \tag{6}$$

where ΔH_f is the measured heat of fusion/gram from the area under the melting endotherm and ΔH_f^0 is the enthalpy of fusion/gram for a 100% crystalline sample. In the case of i-PMP, there have been several reported values for ΔH_f^0 ranging from 65.4 to 118.9 J/g.[34–36] The value of ΔH_f^0 = 65.4 J/g was chosen and used throughout this study for no other reason but to choose a consistent value for calculating the level of crystallinity. The crystallinity was determined by calculating the area under the melting endotherm for the sample using the standard supplied Perkin–Elmer software. Baseline corrections were also done with the supplied software. Instrument calibration was done with indium and tin samples at the same heating rate of 30°C/min.

RESULTS

Resins A

Figure 3 displays the surface morphologies as observed via AFM of the four resin A films, A1–A4, produced at the extrusion conditions listed in

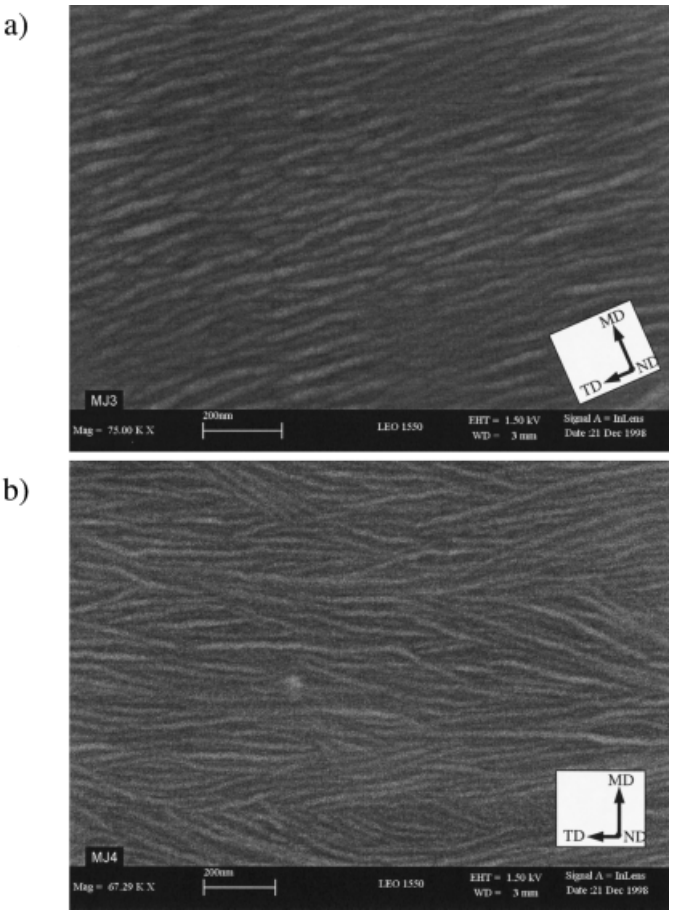

Figure 4 FE–SEM micrographs PMP resin A films: (a) A1; (b) A2. The MD is labeled.

Table II. The lamellar morphologies are observed to be relatively planar and well defined with their long axis principally oriented perpendicular to the MD. There do appear to be a few twisted or tilted lamellae in films A2 and A4, Fig. 3(b,d), respectively, which are indicated by arrows within the figures. As observed by AFM, there are only small observable differences in lamellar twisting between the resin A film morphologies. Figure 4(a,b) displays FE–SEM micrographs of the resin A films A1 and A2, respectively. There is significantly more noticeable twisting/tilting of the lamellae in film A2 [Fig. 4(b)] than in film A1 [Fig. 4(a)]. It is noted that AFM and SEM were utilized as surface techniques in this study, and the bulk film morphology might be different from that of the surface. To address this issue, TEM was performed on two of the resin A films, A1 and A2, after staining with RuO_4. The TEM micrographs are displayed in Figure 5(a,b), respectively. It was found that the A1 lamellae are more planar relative to the A2 lamellae when viewing these films along the TD of the film. Further, due to the thin film thickness (ca. 1 mil) of these extruded films, no distinct skin–core morphological differences were seen in these films or in any films of the other resins (B or C).

As stated earlier, the extrusion setup resulted in planar extensional flow along the MD, thereby promoting uniaxial orientation behavior with respect to the MD. To verify that uniaxial symmetry exists about the MD axis, refractometry was performed to determine the refractive index for all three directions (MD, TD, and ND) of a PMP film. As expected for uniaxially oriented systems, the ND and TD refractive index values were equivalent (ca. 1.4613), while the refractive index along the MD was different (ca. 1.4607). In addition, a WAXS pattern (Fig. 6) was obtained with the X-ray beam parallel to the MD. Further, this suggests that one can use a flat-film X-ray camera to approximate the orientational state of the crystalline phase in the extruded films according to the procedures outlined earlier. In subsequent WAXS patterns for films from resins A–C,

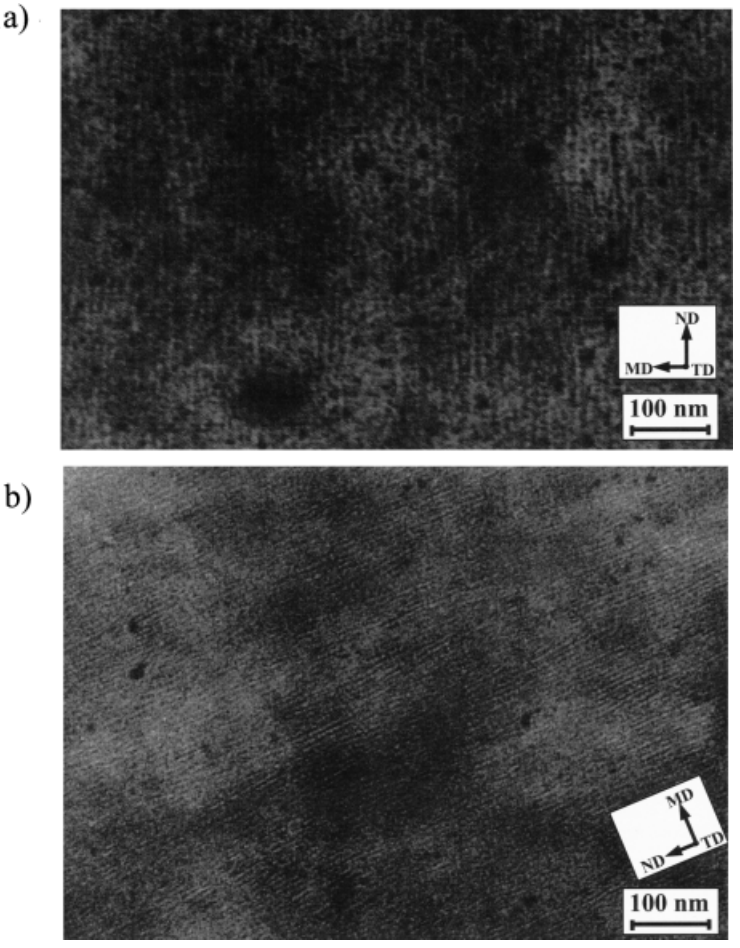

Figure 5 TEM micrographs of RuO_4-stained PMP resin A films: (a) A1; (b) A2. The MD is labeled.

the X-ray beam was along the ND of the extruded film, and the results were utilized to obtain f_c by eqs. (3) and (4). For the resin A films A1, A2, A3, and A4, the WAXS diffraction patterns are displayed in Figure 7(a–d), respectively. In each diffraction pattern, the reader can observe that the (200) reflection

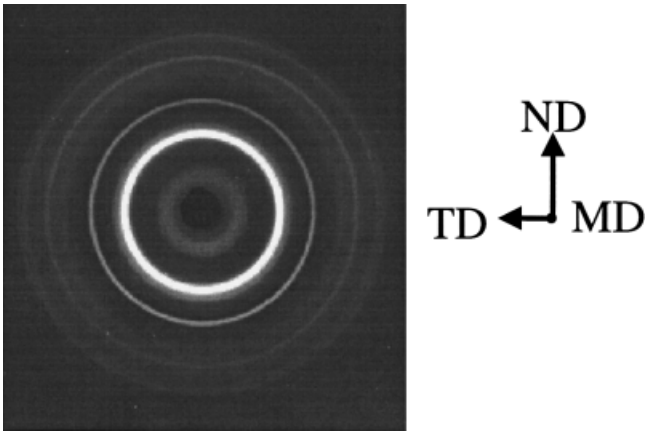

Figure 6 WAXS photograph of an oriented PMP film with X-ray beam parallel to film MD isotropic crystal orientation with respect to the ND of the film.

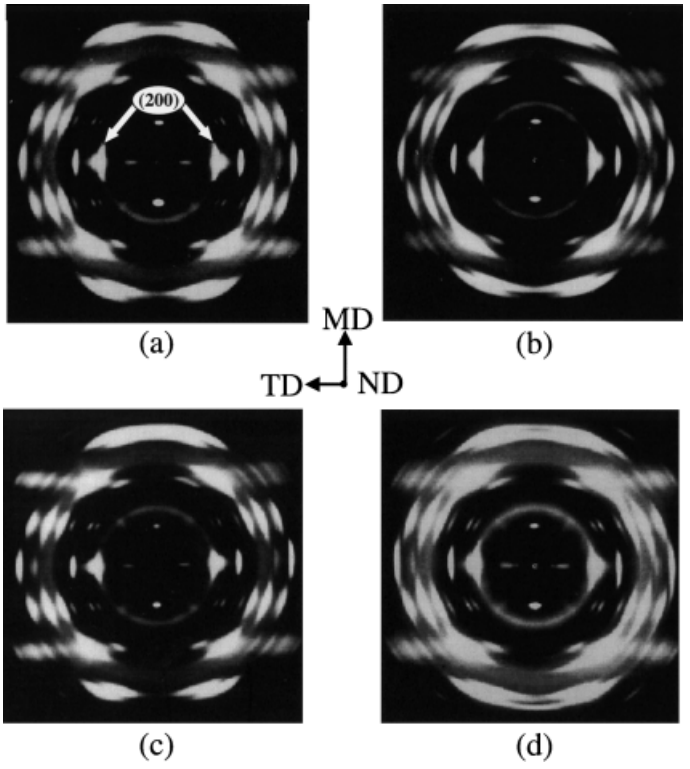

Figure 7 WAXS photographs of resin A PMP films: (a) A1; (b) A2; (c) A3; (d) A4. The MD is labeled. Arrows in (a) indicate the scattering reflection corresponding to the (200) set of planes.

possesses a high degree of azimuthal dependence. In Figure 7(a), the reflection corresponding to the (200) planes (indicated by an arrow) is utilized to calculate f_a and, thus, f_c or the c-axis (chain axis) orientation with respect to the film MD. The crystalline chain orientation, f_c, for each of these films is listed in Table V with other pertinent film properties, and it is clearly indicated that the A1 melt-extruded film is more oriented with respect to MD than is film A2. Further, it is observed that the crystalline orientation values of the resin A films are ranked in the following manner: A3 > A1 > A4 > A2, which is clearly a consequence of the extrusion conditions, as discussed later.

Table V Crystalline Orientation (f_a and f_c), Percent Crystallinity, and Melting Points for the Resin A Films

Sample	$f_{a(200)}$	$f_{c(200)}$	X_c (%)	T_m (°C)
A1	−0.45	0.90	63	229
A2	−0.42	0.84	62	231
A3	−0.46	0.92	60	231
A4	−0.43	0.86	63	230

For the resin A films, the crystalline melting point (T_m) and percent crystallinity (X_c) are also listed in Table V, where both T_m and X_c were determined with the aid of DSC. For the resin A films displayed in Table V, all crystallinities are approximately 62%, while the T_m's are about 230°C. Figure 8 displays a DSC heating scan of the resin A film A1 as well as other DSC heating scans for the resin B film B1 and resin C film C1. Each film (A1, B1, and C1) presented in Figure 8 was melt-extruded under similar conditions. The resin B film and C film results are discussed more extensively later; however, the reader notes that in Figure 8 it is observed that the resin A and C films each possess a single sharp melting endotherm while the resin B film does not. These DSC results are representative of the melting endotherms from other films of the same resin.

Resin B

As shown in Table III, the melt-extrusion conditions utilized to produce the resin B films are

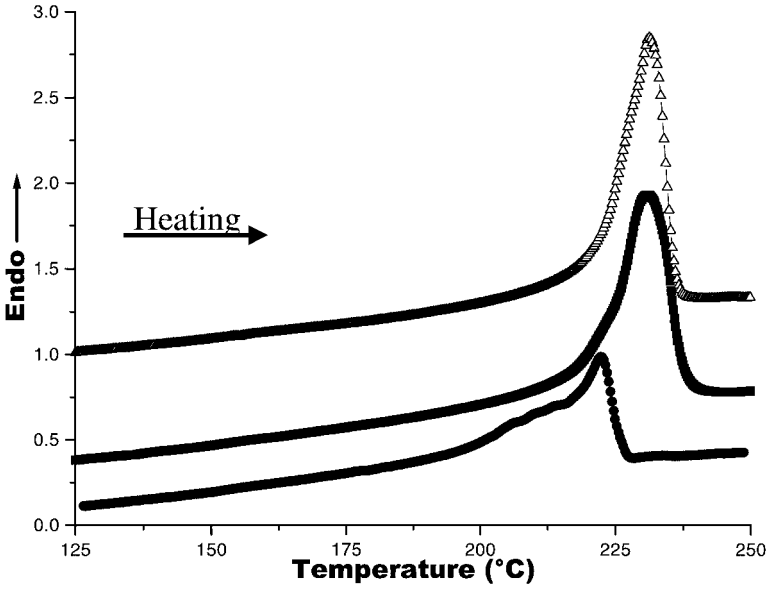

Figure 8 DSC heating scans of PMP films: (—■—) A1, (—●—) B1, and (—△—) C1, utilizing a heating rate of 30°C/min.

analogous to those employed for the resin A films. Upon examination of the WAXS patterns of each film, displayed in Figure 9, it is observed that the azimuthal dependence and, thus, f_c values for the resin B films are also relatively high. Therefore, the resin B films are characterized by relatively

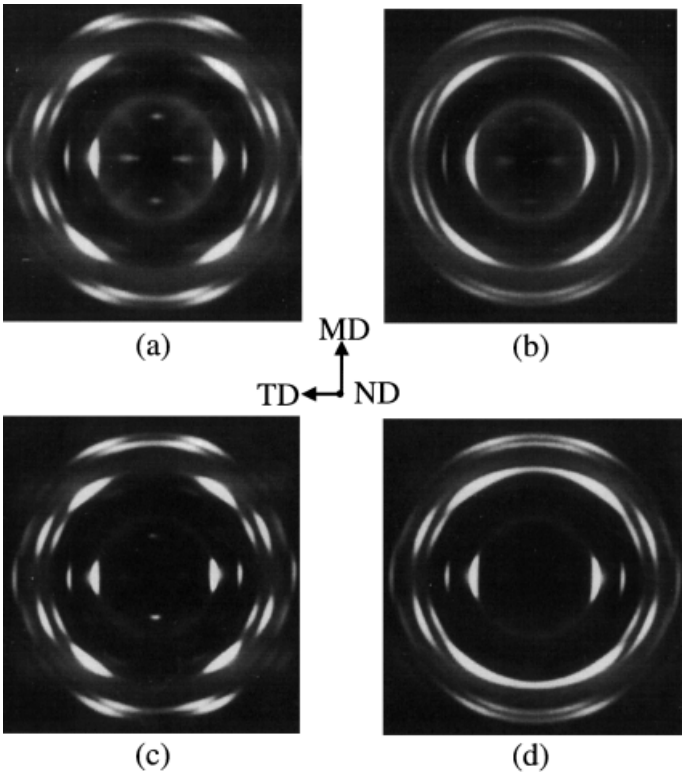

Figure 9 WAXS patterns of resin B PMP films: (a) B1; (b) B2; (c) B3; (d) B4. The MD is labeled.

Table VI Crystalline Orientation (f_a and f_c), Percent Crystallinity, and Melting Points for the Resin B Films

Sample	$f_{a(200)}$	$f_{c(200)}$	X_c (%)	T_m (°C)
B1	−0.42	0.84	42	221
B2	−0.29	0.58	45	223
B3	−0.44	0.88	43	222
B4	−0.41	0.82	40	220

high c-axis alignment with the MD, except for film B2, which has the lowest f_c value of 0.58. The other resin B films (B1, B3, and B4) possess f_c values on the order of 0.84. As shown in Table VI, the resin B film f_c values are ranked in the same order as those of the resin A films, that is, B3 > B1 > B4 > B2. This result is a direct consequence of the differences in the applied melt stress between the different extrusion conditions; for example, condition #3 created a higher extrusion stress state than that of condition #1, regardless of the resin utilized. Note that these results are despite the additional comonomer (ca. 6.5 wt %) present in this resin.

The AFM micrographs of the films B1 and B2 are displayed in Figure 10(a,b), respectively. It is observed in Figure 10(a) that film B1 possesses a planar lamellar morphology, while film B2, displayed in Figure 10(b), is characterized as having

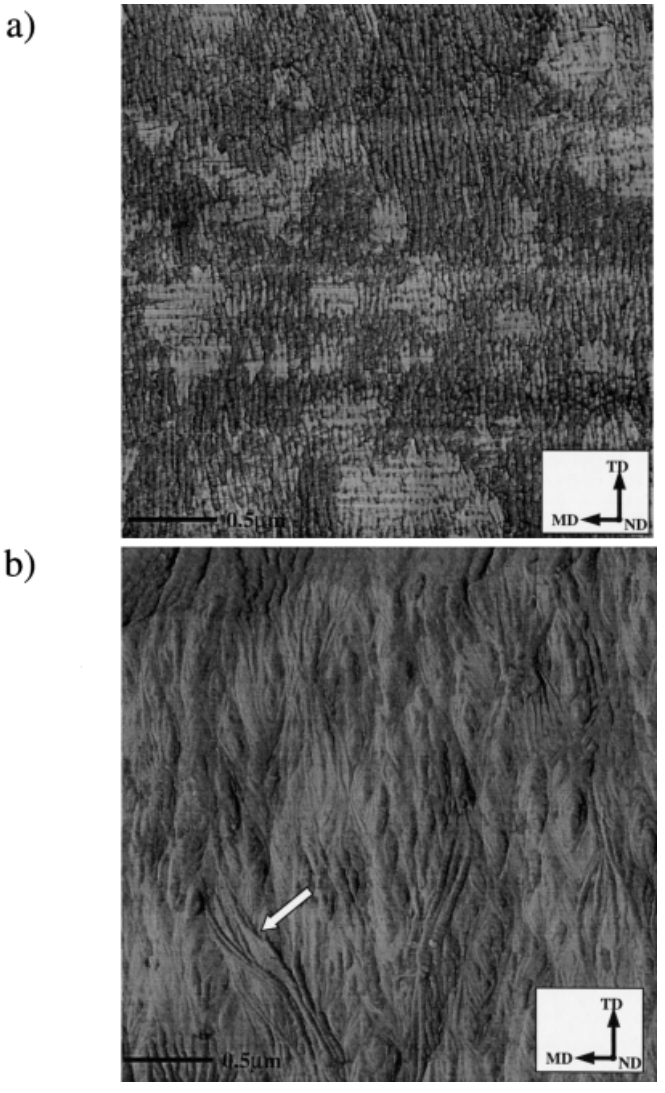

Figure 10 AFM phase images of the resin B PMP films: (a) B1; (b) B2. The MD is labeled. Images are 3 × 3 μm.

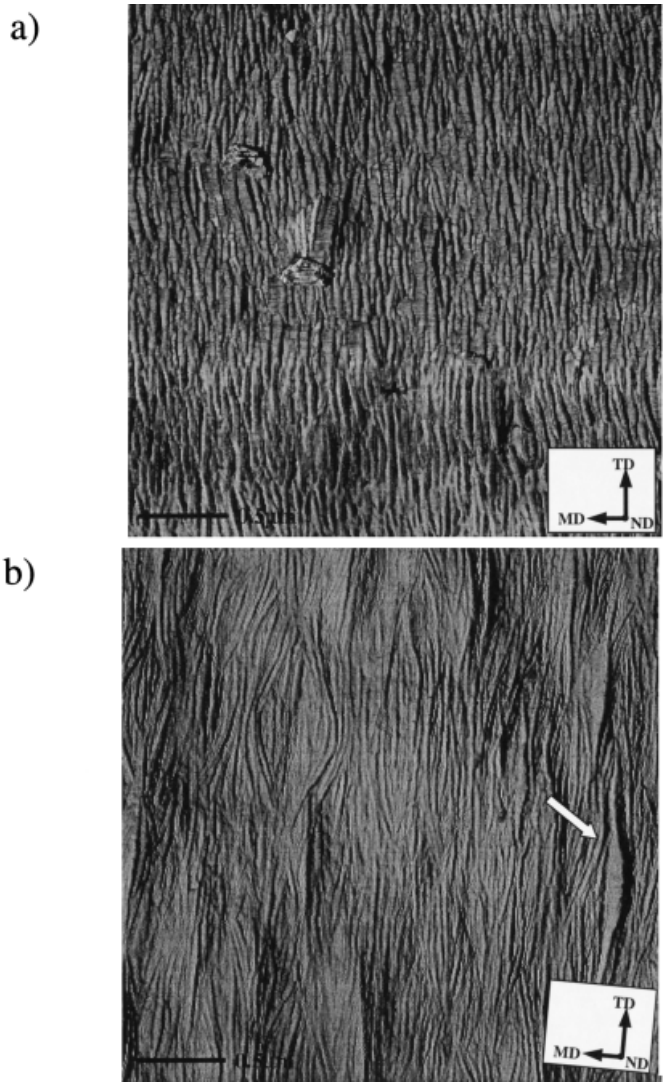

Figure 11 AFM phase images of the resin C PMP films: (a) C1; (b) C2. The MD is labeled. Images are 3 × 3 μm.

a sheaf or fanlike morphology. Films B3 and B4, not shown here, also displayed nearly planar lamellar textures when analyzed with AFM. While TEM was utilized for observing the bulk structure of the resin B films, they are not presented because of their similarity with the corresponding AFM results.

The crystallinity of the resin B films does not appear to change greatly by the varied melt-extrusion conditions. The melting points for the resin B films also do not change under the various extrusion conditions and are presented along with percent crystallinity in Table VI. Assignment of a specific value to the maxima in the melting endotherms may not be precise due to the relative broadness of the melting endotherms for the resin B films (recall Fig. 8).

Resin C

As observed in Table IV, the extrusion conditions used to obtain films C1, C2, and C3 are the same as those used to obtain resin A films A1, A2, and A3. The AFM micrographs of films C1 and C2 are displayed in Figure 11(a,b), respectively, where a morphological change is observed upon comparing the AFM micrograph of film C1 versus film C2. Both films C3 and C5 possessed similar morphologies to film C1 but are not presented here for brevity. In Figure 11(b), film C2 is found to possess evident lamellar twisting, where a single la-

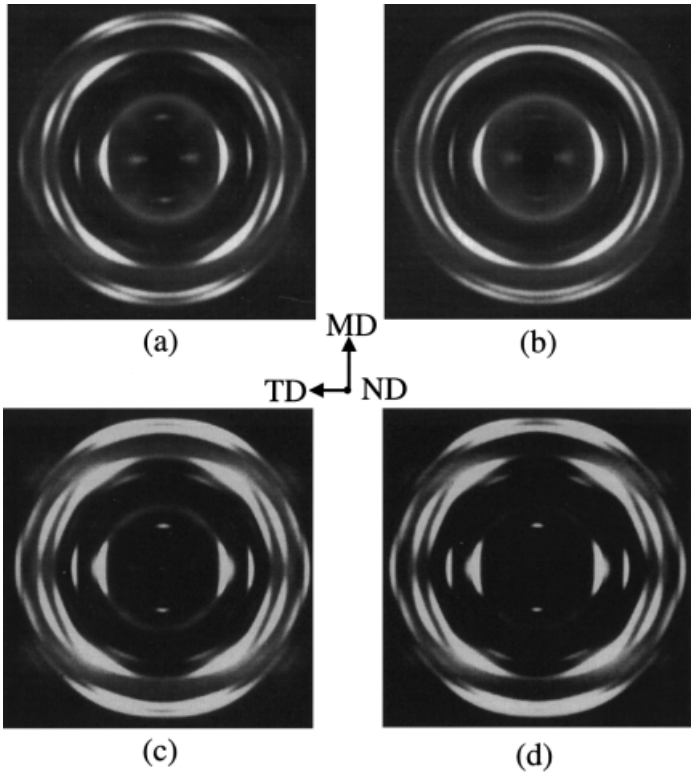

Figure 12 WAXS photographs of resin C PMP films: (a) C1; (b) C2; (c) C3; (d) C4. The MD is labeled.

mella, indicated by an arrow, appears to complete a $\frac{1}{2}$ twist about its long axis. In addition, larger-scale sheaf or fanlike morphologies are evident for film C2 [Fig. 11(b)], similar to the fanlike morphology previously observed for film B2 [recall Fig. 10(b)]. Further, TEM micrographs confirmed that films C1, C3, and C5 possessed a slightly more planar lamellar morphology in the bulk than did film C2.

The resin C film WAXS patterns are displayed in Figure 12. Upon analysis of the (200) reflection, the azimuthal dependence appears approximately the same for films C1, C3, and C5. In contrast, film C2 appears to possess a slightly less azimuthal dependence. Similarly, the *c*-axis orientation of the crystal phase for these films, displayed in Table VII, is found to be approximately the same for the films C1, C3, and C5, while it is lower for film C2.

The resin C films also possessed relatively sharp melting peaks as previously recognized by the data in Figure 8. The processing conditions utilized in this study to produce the resin C films also did not appear to systematically influence the crystallinity or melting point as determined with the aid of DSC. As observed in Table VII, the crystallinities are approximately 63% while the T_m's are about 230°C.

DISCUSSION

Effects of Extrusion Conditions

Upon analysis of the results for a given resin, for example, resin A, it should be clear that the melt-extrusion conditions utilized here affected the

Table VII Crystalline Orientation (f_a and f_c), Percent Crystallinity, and Melting Points for the Resin C Films

Sample	$f_{a(200)}$	$f_{c(200)}$	X_c (%)	T_m (°C)
C1	−0.34	0.68	63	231
C2	−0.23	0.46	64	231
C3	−0.33	0.66	62	229
C5	−0.34	0.68	63	230

morphology and main-chain crystalline orientation (f_c) of these films. In the case of the resin A films, the crystalline orientation values were ranked accordingly: A3 > A1 > A4 > A2, which is a direct result of differences among the process conditions #1, #2, etc., presented in Table II. In terms of the Deborah number, a film possessing a higher f_c was extruded at a higher Deborah (more elastic melt behavior) than was a film possessing a lower f_c. Therefore, the Deborah number (qualitatively) associated with the resin A melt-extrusion conditions (#1, #2, etc.) decreases according to decreasing f_c values (i.e., A3 > A1 > A4 > A2), which is expected upon analysis of the extrusion conditions. Since the viscosity of a polymer melt increases with a decreasing extrusion temperature, a lower melt temperature at the die exit will promote a longer melt-relaxation time and, thus, a higher-oriented melt upon crystallization, for example, film A3 versus film A1. The precursor f_c is also affected by the orientation that can be maintained from the stressed melt into the final product, which is influenced by the how fast and how quickly the melt is crystallized. From these considerations, a larger quench height allows a greater time scale for the melt to relax prior to reaching the quenching ring (lower D_e or more liquidlike behavior). This effect just described accounts for the lower f_c of the resin A film A4 compared against film A1 (condition #4 versus #1). The extrusion speed and line speed can also affect the experimental time in this manner, for example, comparing the resulting films from conditions #2 and #1, where slower extrusion speed/line speed values also lengthen the time it takes for the oriented melt to reach the cooling ring. Recall that the film thickness for this study was maintained at approximately 1 mil (25 μm) and, thus, the extrusion speed and line speed are interdependent upon each other. Film A2 was also a product of the highest thermal energy condition when compared with all other resin A films presented.

As stated earlier, the same melt-extrusion conditions utilized for resin A were employed for resin B. The resin B film f_c values proceed in a similar manner as those of the resin A films; therefore, similar arguments concerning the melt-extrusion conditions can be made, and, thus, qualitatively, the Deborah numbers follow the same trend (i.e., B3 > B1 > B4 > B2). Recognize that the f_c values for the resin A films are higher than comparably extruded resin B films. This suggests that for a given extrusion condition, for example, #1, the resin B precursor was the product of a lower Deborah number than was the resin A film, for example, A1 > B1. This is believed to be a direct result of resin B possessing a lower M_w than that of resin A, as will be addressed later. For resin C films, the f_c results generally deviate from the trends observed in the resin A and B films. This is regardless of the fact that the first three melt-extrusion conditions, #1–#3, are similar to those used for both resins A and B. The exception occurs when comparing the f_c value of film C2 to C1, where the value of f_c for C2 is lower due to the same reason addressed above when comparing extrusion conditions #1 and #2. However, the resin C films, C1 and C3, are characterized by similar f_c values. This suggests that the change in the extrusion temperature from 255°C for C1 to 250°C for C3 was not sufficient enough to strongly influence the melt-relaxation response of the resin C melt for the given experimental time. In fact, film C5 possesses a similar f_c value to that of these two films (C1 and C3) despite that its extrusion condition (#5) is characterized by a higher line speed and extrusion speed with a lower quench height. This lack of an increase in f_c for films C3 and C5 relative to the f_c values of resin A processed under equal conditions is again principally believed to be a consequence of this resin's low M_w.

As introduced earlier in this report, a means to account for the influence of the melt-extrusion conditions on the flow field and, thus, the crystal morphology was first proposed by Keller and Machin.[37] The flat planar lamellae of the resin A films A3 and A1 indicate that these films are products of higher extrusion stress conditions, while those extrusion conditions employed to produce resin A films A4 and A2 are of lower stress. Planar and nonplanar lamellar morphologies were also observed for the resin B and C films. Films B2, B4, and C2 are considered products of lower stress-extrusion conditions in which films B2 and C2 [shown earlier in Figs. 10(b) and 11(b), respectively] possess larger-scale sheaf or fanlike morphologies that are oriented perpendicular to the film MD. Similar larger-scale morphologies previously have been reported for PB-1 blown tubular films by Hashimoto et al.,[38] where these PB-1 fanlike morphologies were also oriented perpendicular to the film MD. Despite these similarities, there is a lack of any visible fibrillar nuclei or row-nuclei (shishes) in the PMP films discussed in this article or our published results on PB-1.

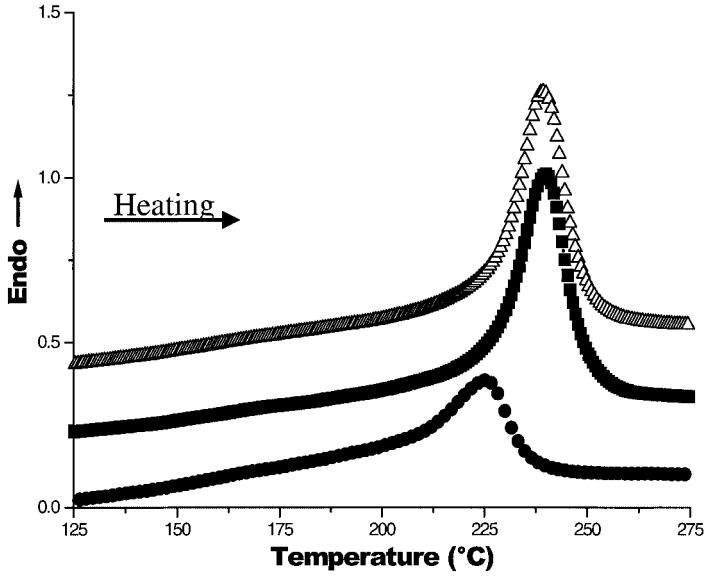

Figure 13 DSC heating scans of the PMP resins utilized in this study: (—■—) resin A; (—●—) resin B; (—△—) resin C. A heating rate of 30°C/min was employed.

The absence of these fibrillar morphologies is of importance because they proposed to nucleate the lamellae as well as to control the level of lamellar twisting/tilting.[15] According to Keller,[39] however, the lack of directly observable shishes or fibril nuclei does not eliminate the presence of so-called "microshishes"[15,16] that represent smaller-scale fibril nuclei that provide for the epitaxial development of lamellar growth preferentially perpendicular to the nucleation sites. Also, these microshishes provide some local connectivity between adjacent lamellae. Thus, they can act to control the level of lamellar twisting/tilting where a greater number of these microshish morphologies would be a consequence of higher extrusion stress conditions, thus resulting in more of a planarlike lamellar texture characterized by preferential *c*-axis orientation. In other words, nucleation from varying levels of "microshish" morphologies, where the amount of these structures is a consequence of the level of extrusion stress, would account for the observed morphological behavior.[16,39]

The morphological features or orientation state did not appear to significantly alter T_m or the crystallinity when comparing films within a specific resin. This suggests that both properties (T_m and X_c) were not greatly affected by the melt-extrusion variables utilized within this work. In fact, both resin A and C films possessed similar crystallinity levels (ca. 62%) and melting points (ca. 230°C). This similarity in crystallinity between resins possessing different MWD values (resin A = 10.3 and resin C = 7.8) differs from previously reported results for HDPE[13] films and iPP[40] fibers. In contrast to the resin A and C results, the resin B films displayed significantly lower levels of crystallinity as well as lower T_m values.

Comparison of Films Extruded from Different Resins but Under Equal Conditions

Recalling that resin B possesses roughly double the comonomer level of that of resins A or C, the lower values of T_m or X_c for the resin B films are easily explained. The comonomer effect on X_c and T_m for each *resin* can be observed in the DSC results presented in Figure 13 (also recall Fig. 8 for the precursors). It is found that the relatively sharp melting endotherm of resin A virtually mimics that of resin C, and both resins possess a melting point of approximately 240°C. In contrast, the melting endotherm of resin B occurs at a lower temperature (226°C), which is a consequence of disruption in chain symmetry due to the additional comonomer.

The higher comonomer content of resin B also influences the temperature at which crystallization takes place upon quenching the quiescent melt. While not displayed here, the nonisothermal crystallization temperature (T_{mc}) for a cooling rate of 30°C/min was observed to be equal to about 199°C for resins A and C; however, it was

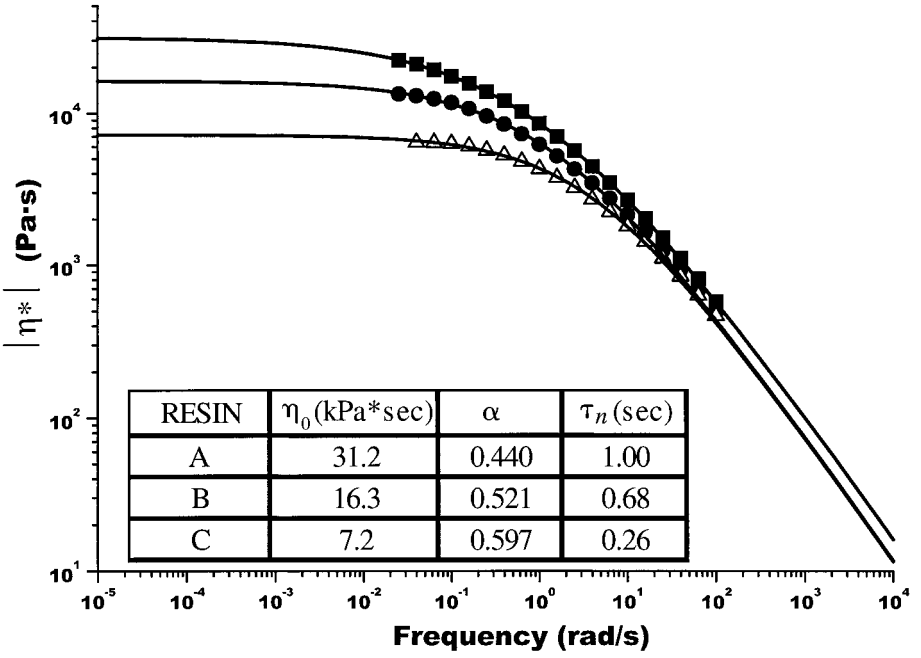

Figure 14 Complex viscosity versus frequency for resins: (—■—) A; (—●—) B; and (—△—) C from this study obtained via dynamic oscillatory shear measurements at 270°C. A table of the CY parameters is included.

depressed to 182°C for resin B. For resin B, greater relaxation of an oriented melt should therefore be possible than if the comonomer level were *similar* to that of A or C (ca. 3.2 wt % decene). A resin that possessed the same M_w and MWD as those of resin B but with a comonomer level of about 3.2 wt % was not available to test this hypothesis. In addition, the resin B films possess f_c values and morphologies that are not drastically different from those of the resin A or C films. In fact, for similarly extruded films (e.g., condition #1 films A1, B1, and C1), the f_c value of film B1 (0.84) is between the higher f_c of film A1 (0.90) and the lower value for C1 (0.68). This finding is more likely a direct consequence of the M_w differences between resins. A similar effect on the crystal orientation was observed in HDPE by decreasing the M_w.[13]

In Figure 14, the complex viscosity data are displayed as a function of frequency for the PMP resins. The viscosity curves were fitted with the three-parameter CY relationship [eq. (1)] and the results are given in Figure 14. The zero shear viscosity (η_0), the relaxation time (τ_n), and the parameter a are also included in the table inserted within Figure 14. Of particular interest among these CY parameters is the relaxation time parameter, τ_n, which for the higher M_w resin A is approximately 1.5 and four times greater than that of resins B and C, respectively. This finding quantitatively confirms the above statement regarding the observed differences in the values of f_c between comparably extruded films from the different resins, for example, samples A1 versus C1. In addition, it provides evidence as to why a more twisted lamellar morphology results for the films from the relatively lower M_w resin versus those films of the relatively higher M_w resin.

The reader may recall that the overall goal of our study was to produce PMP microporous films. Following film extrusion, the next step in this process is for a selected number of these melt-extruded PMP films to be annealed followed by uniaxial stretching parallel to the film MD. The results of these investigations will be covered in a subsequent article.[41]

CONCLUSIONS

Three PMP resins (A, B, and C) possessing differing M_w were studied. Each resin was uniaxially melt-extruded using a number of extrusion variable combinations, resulting in a variety of stacked lamellar morphologies. The relative ex-

trusion stress, as controlled by the melt-extrusion conditions, played a crucial role in the morphological features. At higher stress conditions, more planarlike lamellar conformations were observed, which contrasted the twisted lamellar structures as a result of the lower extrusion stress conditions. In fact, when a resin possessing a relatively fast relaxation time (e.g., resin C) was processed at a low stress condition, superstructure like sheaf morphologies were noted.

It was observed that at 264°C the CY melt-relaxation time of resin C is approximately four times faster than that of resin A, while the relaxation time of resin B is approximately 1.5 times faster than that of A. These melt-relaxation time results are due to the differences in M_w values, where resin C possessed the lowest M_w; resin B, an intermediate M_w; and resin A, the highest M_w of the PMP resins studied. Upon comparison of films from resins A, B, and C, the M_w influence on the morphological features and orientation state was recognized. The films from the higher M_w resin A were generally characterized by flat planar lamellar structures, while the films of resins B or C possessed more visible amounts of lamellar twisting/tilting.

The *c*-axis or main-chain f_c values all suggested preferential alignment with the MD. Upon comparison of films within a resin, the *c*-axis f_c values changed according to the processing parameters, which affected the level of chain orientation in the melt prior to crystallization. There did not appear to be a melt-extrusion parameter that influenced the f_c values more significantly than another *for the process window studied.* It was observed that the extrusion temperature, quench height, and line speed in conjunction with the extrusion speed each affects the resulting film main-chain orientation. Upon contrasting comparably extruded films from different resins, the resin A films possessed f_c values higher than those of the resin B films, which were higher than those of the resin C films. Since the melt-rheological behavior of these PMP resins was strongly dependent upon the M_w, the authors reiterate that both the relaxation response and the process conditions are critical in the structure development upon crystallization. Further, it is believed that the orientation state (e.g., higher versus lower f_c) and morphological features (e.g., planar versus slightly twisted/tilted lamellae) of these PMP films will influence the properties of the microporous membranes made from these melt-extruded films. This will be further explored in the subsequent article addressing these aspects.

The authors would like to thank the Celgard Corp. LLC for their continuing financial assistance for this project as well as the informative discussions that have taken place with them. We would like to thank the late Dr. Andrew Keller for his informative discussions regarding the microshish structures. The authors also thank Stephen McCartney for aiding in the TEM as well as AFM instruction.

REFERENCES

1. Bierenbaum, H. S.; Isaacson, R. B.; Druin, M. L.; Plovan, S. G. Ind Eng Chem Prod Res Dev 1974, 13, 2.
2. Callahan, R. AICHE Symp 1988, 84(261), 54.
3. Sarada, T.; Sawyer, L. C.; Ostler, M. I. J Membr Sci 1983, 15, 97.
4. Chen, R. T.; Saw, C. K.; Jamieson, M. G.; Aversa, T. R.; Callahan, R. W. J Appl Polym Sci 1994, 53, 471.
5. Strathmann, H. Synthetic Membranes: Science, Engineering, and Applications; Bungay, P. M.; Lonsdale, H. K.; de Pinho, M. N., Eds.; Riedel: New York, 1983.
6. Williams, J. L.; Gunther, H.; Peterlin, A. U.S. Patent 89516, 1974.
7. Soehngen, J.; Ostrander, K. U.S. Patent 4257997, 1981, (assigned to Celanese Corp.).
8. Nago, S.; Mizutani, Y. J Appl Polym Sci 1998, 68, 1543.
9. Mizutani, Y.; Nakamura, S.; Kaneko, S.; Okamura, K. Ind Eng Chem Res 1993, 32, 221.
10. Nakamura, S.; Okamura, K.; Kaneko, S.; Mizutani, Y. J Appl Polym Sci 1995, 49, 143.
11. Proceedings of the Robert A. Welch Foundation, XXVI. Synthetic Polymers, Houston, TX, Nov. 15–17, 1982.
12. Celgard Corp. LLC, company product literature.
13. Yu, T. H.; Wilkes, G. L. Polymer 1996, 37, 4675; Erattum 1997, 38, 1503; J Rheol 1996, 40, 1079.
14. Keller, A.; Machin, M. J Macromol Sci Phys B 1967, 1, 153.
15. Keller, A.; Kolnaar, J. W. H. Progr Colloid Polym Sci 1993, 92, 81.
16. Keller, A.; Kolnaar, H. Materials Science and Technology: A Comprehensive Treatment; Wiley: New York, 1997; Vol. 18, Chapter 4, pp 189–268.
17. Kamo, J.; Uchida, M.; Hirai, T. Jpn. Patent 63[1988]–256 712, 1988.
18. Twarowska-Schmidt, K.; Wlochowicz, A. J Membr Sci 1997, 137, 55.
19. Celgard, personal communication.
20. Graessley, W. W. Adv Polym Sci 1974, 16, 1.
21. Graessley, W. W. J Chem Phys 1967, 47, 1942.

22. Hieber, C. A.; Chiang, H. H. Rheol Acta 1989, 28, 321.
23. Hieber, C. A.; Chiang, H. H. Polym Eng Sci 1992, 32, 931.
24. Wilkes, G. L. In Encyclopedia of Polymer Science and Engineering; Kroschwitz, J. I., Ed.; Wiley: New York, 1988; Vol. 14, p 542.
25. Natta, G.; Corradini, P.; Bassi, I. W. R C Accad Naz Lincei 1955, 19, 404.
26. Frank, F. C.; Keller, A.; O'Connor, A. Philos Mag 1959, 4, 200.
27. Choi, C. H.; White, J. L. International Polymer Processing: Fibers and Films; Hanser: Munich, 1998.
28. Choi, C.; White, J. ANTEC Prepr 1997, 228, 2011.
29. Johnson, M. B.; Wilkes, G. L. ANTEC Prepr 1999.
30. Stein, R. S.; Norris, F. H. J Polym Sci 1956, 21, 381.
31. Stein, R. S. J Polym Sci 1958, 31, 327.
32. Stein, R. S. J Polym Sci 1958, 31, 335.
33. For more information, see http://www.metricon.com.
34. Karasz, F. E.; Bair, H. E.; O'Reilly, J. M. Polymer 1967, 8, 547.
35. Charlet, G.; Delmas, G. J Polym Sci Polym Phys Ed 1988, 26, 1111.
36. Charlet, G., Ph.D. Thesis, Department of Chemistry, McGill University, Montreal, Canada, 1982.
37. Keller, A.; Machin, M. J. J Macromol Sci-Phys B 1967, 1, 41.
38. Hashimoto, T.; Todo, A.; Murakami, Y. J Polym Sci Polym Phys Ed 1977, 15, 501.
39. Keller, A., personal communication.
40. Misra, S.; Lu, F. M.; Spruiell, J. E.; Richeson, G. C. J Appl Polym Sci 1995, 56, 1761.
41. Johnson, M. B.; Wilkes, G. L., in preparation.